Ultrathin $Cu(In,Ga)Se_2$ solar cells with passivated back interface: a comparative study between Mo and In_2O_3:Sn back contacts

Yong Li[1], Guanchao Yin[2*], Ye Tu[2], Setareh Sedaghat[1], Yao Gao[1], Martina Schmid[1*]

[1]Faculty of Physics, University of Duisburg-Essen & CENIDE, Forsthausweg 2, 47057 Duisburg, Germany
[2]School of Materials Science and Engineering, Wuhan University of Technology, Luoshi Road 122, 430070 Wuhan, China
** Corresponding authors:*
Martina Schmid, E-mail: martina.schmid@uni-due.de;
Guanchao Yin, E-mail: guanchao.yin@whut.edu.cn.

Abstract:
Point contact passivation layers have been proven beneficial in most solar cells (SC). However, the latest theoretical simulations suggested that a high back contact recombination velocity S_b can also be beneficial in ultrathin CIGSe ($Cu(In, Ga)Se_2$) SCs, if they have a relatively high back potential barrier height E_h. SCAPS simulations predicted that a high S_b will deteriorate the SC efficiency *Eff* when E_h is in the range of 0 - 0.17 eV (Ohmic contact). Yet, when E_h is greater than 0.17 eV (Schottky contact), a high S_b can also diminish the current limitation arising from the back Schottky diode, since it has a reverse direction to the main p-n junction. Therefore, a high S_b can support the carriers in passing the Schottky barrier via recombination, thus enhancing the cell performance. This work aims to verify the simulation prediction in practical experiments. To achieve different S_b, we fabricate SiO_2 passivation layers with point contacts of various dimensions by nanosphere lithography. The passivation effects were studied comparatively on Mo and ITO (In_2O_3: Sn) back contacts. The emphasis is on E_h, which is marginal for Mo but acts Shottky-like on ITO. We show that for Mo-based solar cells, the E_h is trivial, hence a high S_b (without SiO_2 passivation) deteriorates the efficiency. In contrast, on ITO the reference sample without SiO_2 shows less current limitation than the passivated ones, implying that a high S_b improves the *Eff*. Comparing the differences of SiO_2 on Mo and ITO back contacts in experiments, with the contrastive behavior of S_b on Ohmic and Schottky contact in simulation, we conclude that E_h decides about the role of S_b in ultrathin CIGSe SCs. Those findings deepen the understanding of the Schottky back contact and pave the way for future optimization of bifacial semitransparent ultrathin CIGSe SCs.

Keywords: Ultrathin CIGSe solar cells, back interface passivation, point contact, Schottky and Ohmic contact, back potential barrier

1 Introduction

CIGSe ($Cu(In,Ga)Se_2$) thin-film solar cells have demonstrated their enormous potential in the photovoltaic (PV) market with an efficiency beyond 23% on small areas.[1] Apart from the high conversion efficiency, CIGSe solar cells offer unique advantages, such as short energy payback time, compatibility with curved-surface substrates, great tolerance to non-ideal environment, etc..[2-6] Despite great progress has been achieved in the last decades, a lower cost-to-efficiency ratio is constantly being pursued in CIGSe solar cells, aiming at their large-scale deployment. Recently, ultrathin CIGSe solar cells, namely with a sub-500-nm absorber, have attracted extensive attention.[7] The two major advantages of ultrathin solar cells are the reduction of rare material consumption and the resultant rise of production throughput. Those benefits can

address the concern of indium scarcity and manufacturing cost simultaneously. However, ultrathin CIGSe solar cells are suffering from relatively poor performance with the highest efficiency of 15%,[8] due to the common challenges of insufficient light absorption (optical effect) and back interface recombination (electrical effect). This work emphasizes the electrical recombination characteristics of ultrathin CIGSe solar cells as a central aspect to understand cell performance and optimize the design.

Generally, back surface recombination refers to carrier annihilation at the interface of CIGSe/back contact.[9] Comparing to the 2 μm absorber counterparts, back recombination is particularly severe for ultrathin CIGSe solar cells. The reason is a high concentration of photogenerated carriers in the vicinity of the CIGSe/back interface, where also the trap density is high, naturally activating the interface recombination. In order to address this effect, enormous efforts have been devoted to passivate the CIGSe/Mo interface.[10-18] For instance, inserting point contact nanostructures made of dielectric materials (e.g. SiO_2, Al_2O_3) with local openings between CIGSe/Mo was proved a practical and effective way. It was deduced that the point contacts contribute to back interface passivation by lowering the interface state density.[19] Line contacts with SiO_2 or Al_2O_3 also showed promising results on Mo substrates.[20] For Al_2O_3, the formation of fixed negative charges may also contribute to field passivation effects.[12, 21] In addition, the dielectric materials have a lower refractive index than Mo over a large wavelength range and hence increase the back reflectivity of CIGSe/Mo significantly, which will further benefit the cells in terms of enhanced light absorption.[22, 23]

Alternatively, ultrathin CIGSe solar cells can also be fabricated on TCOs (transparent conductive oxides), which are inherently transparent from visible to near-infrared wavelength range [24, 25]. In this way, the parasitic absorption loss in Mo is circumvented and the unabsorbed light after the first pass through the absorber may be further utilized.[26] The transparency of the back contact opens up many distinct applications such as top cells in tandem configuration, bifacial semitransparent solar cells, or photovoltaic windows.[27, 28] However, due to the work function mismatch between CIGSe and TCO, solar cells on TCOs typically have a Schottky-like back contact, which leads to an inferior cell performance compared to the ones on Mo forming a quasi-Ohmic back contact via interfacial $MoSe_2$.[29, 30] Interestingly, our recent theoretical study predicts that a passivated back interface (reduced recombination velocity S_b) may harm CIGSe solar cells which have Schottky back contacts.[31] This poses a sharp contrast to cells on Mo, where passivation reduces the back contact recombination, increases the interface reflection and thus enhances the efficiency.[31] For a deeper understanding how a passivated back interface deteriorates cells with a Schottky back contact, further research is needed, in particular on TCO back contact. Various explorations have been conducted for solar cells on Mo already, yet most work was limited to demonstrate the beneficial effects of passivation experimentally. The relevant passivation mechanism requires further identification, especially under the fact that CIGSe/Mo is a quasi-Ohmic back contact with a relatively low back potential barrier E_h rather than an ideal Ohmic contact.

In this contribution, we firstly show the different experimental passivation effects of SiO_2 point contacts on Mo and ITO (In_2O_3:Sn) substrates comparatively. To understand the controversial influences of the same SiO_2 passivation layer on different back contact materials, we fall back to the SCAPS theoretical calculations. We then present simulations for solar cells with E_h of 0 and 0.2 eV to demonstrate the two extreme conditions of ideal Ohmic and Schottky back contact, respectively. A varied recombination velocity S_b is used to simulate the passivation effects in practical experiments. The simulated temperature-dependent current-voltage characteristics $j_{net}V(T)$ are compared with the experimental results. In order to decipher the

differences of passivation effects on Mo and ITO, the decisive role of E_h is highlighted.

2 Experiments and Simulations

SiO_2 point contact fabrication: Nanosphere lithography is employed to prepare SiO_2 point contact nanostructures. We use polystyrene (PS) nanospheres as a sacrificial mask, which has been demonstrated feasible and applicable in previous work for preparing point contact nanostructures.[9] Therefore, a commercially available latex solution of PS spheres, with a diameter of 1500 nm in our case, is combined in a volume ratio of 1:1 with a second solution. This latter one consists of 10 µl H_2SO_4 (98%) mixed with 1 ml of ethanol (containing 1 vol.% styrene). The complete solution is subsequently dispersed atop the surface of deionized water and forms a monolayer of closely-packed PS spherescase. By sucking out the water, the PS spheres are transferred onto Mo or ITO substrates as shown in Figure 1 (a). Subsequently, the PS spheres are etched by O_2 plasma treatment at an overall pressure of 0.2 mbar and a power of 240 Watt. The etching time is optimized at 22 minutes, after which the diameter of the PS spheres is reduced to 600 nm, see Figure 1 (b). Next, 50 nm SiO_2 is evaporated via tungsten boat heating SiO_x powder under O_2 gas flux (Figure 1 (c)). No additional heating is used for the substrates in all those preparation processes. Finally, the PS nanospheres are lifted off by a treatment in ultrasonic bath using toluene for 20 minutes. Remaining is the SiO_2 point contact layer on Mo or ITO substrate (Figure 1 (d)). More fabrication details can be found in reference.[9]

Solar cell growth: 300 nm ITO is sputtered on alkali-free (< 0.3% alkali content) Corning glass 7059 substrates. The as-prepared ITO has a sheet resistance around 20 Ω/sq, which will drop to < 10 Ω/sq after the heat treatment during CIGSe co-evaporation. Mo substrates are purchased from Saint Gobain Company, with a Na barrier layer between the glass and Mo. For the absorber fabrication, Mo and ITO substrates with and without SiO_2 point contact passivation layer are loaded into the PVD (physical vapor deposition) chamber in the same batch, and a standard 3-stage co-evaporation process was employed to fabricate the CIGSe absorbers.[32] To maintain the conductivity of ITO, a low substrate temperature of 450 °C is adapted for the 2nd stage. After the 3rd stage, the substrate temperature is decreased to 360 °C for post-deposition treatment with 2 mg NaF (around 3.4 nm thick). After the absorber growth, 60 nm CdS is deposited by CBD (chemical bath deposition) at 60 °C for 8 minutes. Subsequently, an 80 nm thick intrinsic ZnO and a 300 nm thick ZnO:Al (AZO) layer are coated by sputtering at a substrate temperature of 120 °C. Following is the evaporation of 10 nm Ni / 2000 nm Al grid fingers for carrier collection. Finally, the samples are mechanically scribed into 1 cm x 0.5 cm small cells for electrical characterization.

Characterization: A LEO 1530 scanning electron microscope (SEM) is employed to characterize surface and cross section morphologies of the samples. X-ray fluorescence (XRF) spectroscopy is applied to determine composition and thickness of the CIGSe absorbers. Thickness, [Cu]/([Ga]+[In]) and [Ga]/([Ga]+[In]) ratio are identified to be 450 nm, 0.80 and 0.31, respectively. In order to evaluate the performance, light current density - voltage ($j_{net}V$) curves are measured under standard test conditions (25 °C, AM1.5, 1000 W/m^2). In the $j_{net}V$ measurements, a black-painted sample holder is used to avoid reflection effects from the back. Additionally, the temperature-dependent current density - voltage ($j_{net}V(T)$) measurements are performed in the range from 150 - 300 K in an enclosed liquid helium cryostat, with the thermal sensor mounted atop the sample.

SCAPS simulation settings: To simulate the passivation effects in the ultrathin CIGSe solar cells, SCAPS simulations are used,[33-36] and different recombination velocities S_b are set at the

back interface. The S_b for electrons and holes were set equal. According to the transport equation for recombination current density $j_{re} = S_b*D_p = s_p*v_{th}*N_t*D_p$, (where S_b is the recombination velocity, D_p the excess carrier density (holes here), s_p the hole capture cross section, v_{th} the thermal velocity and N_t the trap state density), it is equivalent to vary S_b and N_t in SCAPS simulation.[37] In the experiments, the defect density N_t was decreased at the passivated area while it remained unchanged at the openings of the point contact layer, so the overall quantity of the defect states Q_t at the back interface should be reduced by the SiO_2 passivation. Therefore, S_b in this contribution actually represents an effective recombination velocity, as S_b reflects the variation in Q_t at the back interface. For the settings of SCAPS simulations, based on our previous work in reference (a simplified three layered homojunction),[31] the model was further elaborated to fit with the experimental results in this work. All the simulation results presented in this work were obtained via the elaborated model, which is constructed of Back contact/CIGSe/ODC/CdS/i-ZnO/AZO layers, where ODC stands for ordered-defect-compound, AZO for ZnO: Al and i-ZnO for intrisic ZnO. Detailed settings of each parameter are listed in Table S3.

3 Results and Discussion

Figures 2 (a) and (d) show the top views of the SiO_2 point contact passivation layers on Mo and ITO, respectively. The holes, highlighted with the yellow dotted circles, are the openings that allow the transport of carriers towards the back contact. They follow the periodicity of the initially closely-packed PS nanospheres with a hexagonal array and a pitch of 1500 nm. After SiO_2 deposition, a single point contact has a diameter of 450 nm, indicating the ratio of the point contact openings is 22% (78% area is covered by SiO_2 insulator). To investigate the compatibility of the SiO_2 layers with the absorber and ITO in the solar cells, cross-sections of complete devices without and with SiO_2 are shown in Figure 2 (b)-(c) and (e)-(f), respectively. It is observed that for both Mo and ITO, the absorber exhibits similar large grains, no matter if point contact nanostructures are present or not. The grain height is comparable to the absorber thickness despite the low substrate temperature of 450 °C during the CIGSe growth. More importantly, the absorber shows a conformal growth on the SiO_2 point contact layers with full penetration to the back contact in the point contact openings. The morphologies feature that a good adhesive contact is formed between the absorber and the back contact.

To evaluate the passivation effects in the ultrathin CIGSe solar cells, Table 1 summarizes the PV parameters measured under AM1.5 solar spectrum. On Mo, j_{sc} (short circuit current density) exhibits a pronounced increase by nearly 3 mA/cm^2 after passivation (from 25.3 to 28.2 mA/cm^2). Simultaneously, V_{oc} (open circuit voltage) remained unchanged and FF (fill factor) was enhanced moderately. As a result, the efficiency improves from 9.5 to 11.1%, corresponding to a relative enhancement of 16%. The evolution of efficiencies on Mo is broadly consistent with previous reports, and two major factors are responsible:[9] Firstly, the SiO_2 passivates the CIGSe/Mo interface by lowering the recombination velocity S_b and thus increases the collection efficiency of the photogenerated carriers. Secondly, the low refractive index of SiO_2 improves the interface reflectivity of CIGSe/Mo, redirecting the light not absorbed after the first pass back into the absorber and thus contributing around 0.9 mA/cm^2 photogenerated current density (see supporting information Table S1). Mo_bare and Mo_passivated exhibit overlapping Ga grading profiles towards the back contact (see supporting information Figure S1), indicating that SiO_2 has a marginal effect on the depth distribution of the CIGSe components. Therefore, it is inferred that the electrical passivation benefit in Mo_passivated is the dominant reason for its j_{sc} enhancement, being attributed 2 mA/cm^2 increase.

In contrast, the cells on ITO substrate exhibit an inverse trend compared to Mo: ITO_passivated shows inferior performance than ITO_bare. Inserting SiO_2 passivation layers deteriorates V_{oc} and FF from 597 to 574 mV and 60 to 58%, respectively. Since the SiO_2 layer only enhances j_{sc} by 0.3 mA/cm^2, while the improved back reflectivity at the CIGSe/ITO interface already contributes 0.2 mA/cm^2 (supporting information Table S1), the effect of reduced back recombination on the carrier collection is marginal. Overall, on ITO the passivation layer leads to a drop in cell efficiency from 9.5 to 9.0%. To confirm that the differences on Mo and ITO relate to the presence of a SiO_2 passivation layer in general rather than to the point contact opening ratio, we have also tried 8% and 40% SiO_2 coverage on both substrates. Compared to the reference samples, the PV parameters of the passivated ones show a similar trend as those depicted in Table 1 (see supporting information Table S2). The SiO_2 passivation is beneficial for a back contact made from Mo while it is detrimental for ITO. Therefore, we deduce that the reduced back contact recombination plays a different role in Mo-based and ITO-based ultrathin CIGSe cells. Meanwhile, we notice the FF of the ITO-based solar cells is generally lower than for the Mo-based ones, which is induced by the higher R_s of the devices, as the sheet resistance of the ITO layer is around 10 Ω/□ while for Mo it is only 0.5 Ω/□.

In Figure 3 (a), the black line illustrates the band diagram of the cell with E_h = 0 eV. The equivalent circuit is simplified without considering shunt and serial resistances, represented as the basic circuit in black in Figure 3 (b). j_{ph} means the photogenerated current density in the solar cell's main p-n junction, V_D and j_D are the voltage and current at the main diode, respectively. j_{net} stands for the net current density flowing through the circuit. In addition, the red dotted line in Figure 3 (a) presents the band diagram of a solar cell with E_h = 0.2 eV, and the equivalent circuit can be seen in Figure 3 (b): the additional diode drawn in red simulates the Schottky back contact diode with a reverse direction compared to the main black diode. V_s and j_s represent the voltage and current upon the Schottky diode.

Figure 4 (a) presents the simulated $j_{net}V$ curves for the Ohmic contact solar cells dependent on S_b. As we expect, a higher S_b slightly deteriorates the cell performance by decreasing all PV parameters (the arrow shows the direction of increasing S_b).[9, 38] The reason is that an increased back recombination induces a loss of photogenerated carriers during the collection process. Therefore, the back recombination not only decreases j_{sc} at zero bias but also V_{oc} and FF. Such evolution trend is consistent with our experimental results of cells on Mo, as shown in Figure 4 (b). The black line corresponds to the bare solar cell without SiO_2, (Mo_bare) exhibiting an inferior $j_{net}V$ curve compared to Mo_passivated shown in red. We notice the net forward current j_{net} in the first quadrant is more restrained after passivation. The origin is an increase in R_s from 0.6 to 1.7 Ωcm^2 with the insertion of SiO_2. Generally, R_s is more likely to influence the $j_{net}V$ curve when the forward j_{net} is high in the main diode, corresponding to the first quadrant here. In contrast, in SCAPS simulation, the $j_{net}V$ results take no R_s or R_{sh} into account. One major deviation between Figure 4 (a) and (b) is the V_{oc} difference. In the simulated $j_{net}V$, the lower S_b exhibits a more significant V_{oc} enhancement than in experiments. The main reason is that the E_h of Mo-based solar cells is not 0 eV, but closer to 0.1 eV as shown in Figure S2 (a). We also notice the j_{sc} enhancement of Mo_passivated is higher in experiments than in the simulations. That is because the optical benefit (absorption increment from the inserted low refractive index SiO_2 layer) is not being considered in SCAPS simulations. As a shortcoming in SCAPS simulations, we only put the electrical variations into the simplified simulation model. The optical increment introduced by the SiO_2 layer can be simulated by e.g. RefDex,[39] as shown in supporting information Table S1.

In the case of Schottky contact solar cell, however, a higher S_b improves the $j_{net}V$ characteristics as shown in Figure 4 (c). The higher S_b relaxes the current limitation of the Schottky back diode, as the direction of the Schottky diode is opposite to the CdS/CIGSe main junction. In view of the carrier collection process, the Schottky back contact is a barrier for the holes to pass. With a higher S_b, the holes can annihilate at the interface supporting the flow of the current.[37] Correspondingly, V_{oc} and FF improve continuously for cells with Schottky contact when S_b increases. Figure 4 (d) plots the corresponding experimental $j_{net}V$ curves of the solar cells on ITO. In this case, the un-passivated cell (ITO_bare, black line) with a higher S_b exhibits a better PV performance than ITO_passivated. The red line of ITO_passivated shows a slightly suppressed j_{net} in the first quadrant for similar reasons as on Mo.

Coming back to the simulations in Figure 4 (a) and (c), the two E_h values of 0 and 0.2 eV are chosen as two extreme example conditions for an explicit comparison and discussion. If we vary E_h in smaller steps, there should be a turning point E_t (separation value): When E_h of the CIGSe solar cell is higher than E_t, a higher S_b will be favorable for its PV performance (here we refer to it as Schottky case). On the contrary, when E_h is lower than E_t, the higher S_b will be detrimental for the solar cell (we refer to it as Ohmic case). Based on this, we simulate the solar cell characteristics with continuously varying E_h in the range from 0 - 0.5 eV, and find E_t for the ultrathin CIGSe solar cell to be 0.17 eV, as shown in the supporting information Figure S2. Therefore, basing on the *Eff* turning point, we define $E_h < 0.17$ eV as Ohmic contact and $E_h >$ 0.17 eV Schottky contact. In contrast to the simulations shown in our previous work,[31] which were calculated based on the simplified homojunction model [31], the derivation of E_t in the Table S3 used a more representative structure of the CIGSe solar cell with back contact/CIGSe/ODC/CdS/i-ZnO/AZO (ODC means ordered vacancy compound).

Generally, recombination current density j_{re} and the thermal emission current density j_{th} are two independent ways to describe the carriers passing the back interface.[37] Recombination current density j_{re} represents the part of the current consisting of electrons and holes captured by the trap states and annihilated there. As mentioned earlier, j_{re} can be expressed as $j_{re} = S_b * \mathrm{D_p} = \mathrm{s_p} * v_{th} * N_t * \mathrm{D_p}$. Therefore, j_{re} is sensitive to the passivation as it is proportional to N_t.[37] Meanwhile, the thermal emission current density j_{th} describs the part of current consisting of electrons or holes surpassing the energy barrier E_h via thermal emission. j_{th} can be expressed as $j_{th} = A' * T^2 * exp(-qE_h/k_BT)$, where A' is the effective Richardson constant, T the temperature and q/k_BT the reciprocal of the thermal energy.[37] Therefore, j_{th} is strongly dependent on the temperature T and barrier height E_h, while j_{re} is more likely affected by N_t or S_b, respectively (The thermal velocity is only weakly dependent on the temperature, resulting from $v_{th} = \sqrt{k_BT/m}$, with k_BT being the thermal energy and m the hole mass). Overall, the net current j_{net} equals to the sum of the thermal emission current j_{th} and the recombination current j_{re}.

To study the influence of temperature and passivation on the $j_{net}V$ properties of the solar cells, Figure 5 shows the temperature-dependent $j_{net}V$ curves of four representative samples. For Mo_bare (Figure 5 (a)), when the temperature drops to ≤ 180 K, the $j_{net}V$ curve shows suppressed current in the first quadrant. It implies that for temperatures equal or below 180 K, the electrons' thermal energy is not high enough to surpass the barrier, hence j_{th} decreases tremendously and j_{net} appears suppressed, thus a roll-over effect shows up [40]. In comparison, for Mo_passivated (Figure 5 (b)), the contribution of recombination current is enormously reduced by the SiO_2 point contact layer and most current originates from j_{th}. Therefore, j_{net} appears suppressed at 240 K already. In other words, because j_{re} is diminished by the SiO_2 passivation layer, j_{net} dominated by thermal emission is more easily suppressed at relatively

higher temperatures, hence the roll-over shows up earlier during the process of temperature decrease.

On the other hand, ITO_bare in Figure 5 (c) shows no obvious roll-over in the range from 150 - 300 K. The roll-over only appears when the temperature is further decreased to 130 K (not shown here). It indicates a relatively high part of recombination current (compared to Mo_bare) and j_{net} did not appear suppressed even when the temperature is as low as 150 K. Nevertheless, ITO_passivated shows a roll-over at 240 K (Figure 5 (d)), similar to Mo_passivated. This tells us that j_{re} in ITO_passivated has been severely reduced by the SiO_2 alike on Mo, hence j_{net} is suppressed at 240 K. Through the comparison of the temperature when the roll-over in the $j_{net}V$ curve shows up, we conclude that the SiO_2 point contact layer passivates both CIGSe/Mo and CIGSe/ITO interfaces. The contribution of j_{re} (or recombination velocity S_b) is decreased in both cases, which also explains the suppressed j_{net} in the first quadrant of Figures 4 (b) and (d).

To further demonstrate the different influences of recombination on Ohmic and Schottky contact, we simulate $V_{oc}(T)$ curves for various S_b and extract experimental $V_{oc}(T)$ for ultrathin solar cells with and without SiO_2 passivation as plotted in Figure 6. In the $V_{oc}(T)$ curves, the activation energy E_a can be derived from the linear extrapolation towards 0 K, as shown by the dashed lines. E_a equals the bandgap E_g for ideal Ohmic contact and $E_g - E_h$ for Schottky back contact.[41]

We firstly look at the simulated results. Figure 6 (a) represents the case of Ohmic back contact. We observe an E_a of 1.18 eV, which is independent of S_b. Meanwhile, for the device with a Schottky back contact showing non-negligible E_h (Figure 6 (b)), E_a drops below E_g (1.1 eV in our simulation), as $E_a = E_g - E_h$. From fitting the figure, E_a on Schottky back contact is only 0.97 eV. In addition, a higher S_b leads to a larger E_a, indicating a smaller effective E_h. This indicates a higher S_b can assist the hole transport towards the back contact, diminishing the blocking effect of E_h for the current. Overall, unlike on Ohmic contact devices, the simulations imply that a higher S_b is favorable in the cells with Schottky back contact.

Moving forward to the experimental $V_{oc}(T)$ results shown Figure 6 (c)-(d), we firstly find that E_a is lower for the passivated cells compared to the bare references on both substrates. Secondly, E_a is overall larger on Mo (> 1.14 eV) than on ITO (< 1.14 eV). It confirms two points: 1) Both CIGSe/Mo and CIGSe/ITO are non-Ohmic contacts; they have nonzero E_h. 2) Ultrathin CIGSe solar cells on ITO have a higher E_h than those on Mo. More specifically, on ITO, the SiO_2 passivation layer leads to a higher E_h thus a lower E_a, which is consistent with the theoretical demonstration that a smaller S_b means a stronger blocking effect for the solar cells with a Schottky back contact E_h. Also, that SiO_2 is beneficial on Mo while detrimental on ITO was decided by the E_h value at the back contact. Besides, a notable difference between the simulation and experiment is that E_a is independent of S_b in the simulated cell with Ohmic contact (Figure 6 (a)), whereas it reveals a dependence in experiments on Mo (Figure 6 (c)). The reason is a non-negligible E_h also for the CIGSe solar cells on Mo, for which the contact of CIGS/Mo is typically referred to as quasi-Ohmic contact instead of Ohmic contact.[42-44]

From the $V_{oc}(T)$ comparison above, it has been revealed that the back interface passivation has a double-sided effect on the photovoltaic properties of ultrathin CIGSe solar cells. On the one hand, passivation enables lower recombination of photogenerated carriers and hence benefits the cell performance. On the other hand, passivation aggravates the blocking of forward current through the back Schottky diode, which deteriorates the cell with a Schottky back contact. For

the solar cells on Mo, due to E_h being small and the resultant current blocking effect marginal, the favorable effect dominates over the adverse one. Therefore, in addition to optical benefits brought by the passivation layer, introducing a SiO_2 passivation layer raises the performance of the ultrathin CIGSe solar cells on Mo. In contrast, for the cells on ITO, the back potential barrier E_h and the resultant current blocking effect are not negligible. The current blocking effect dominates, and a back interface passivation tends to deteriorate the cell performance as the blocking behavior is reinforced.

Finally, on Mo substrates, regarding the absence of V_{oc} enhancement after back passivation shown in Table 1, it should be particularly interpreted. One reason is the steep back Ga grading in our samples (See supporting Figure S1). It repels photogenerated electrons away from back contact and thus restrains the back recombination, which acts similarly to passivation. Exactly because of this, back interface passivation will bring a reduced beneficial effect on ultrathin cells with a high Ga grading. More importantly, due to the absorbers being prepared at a quite low temperature in this work (compared to the generally used 565 °C in reference 8, our 450 °C is relatively low), it is speculated that the interfacial $MoSe_x$ was not formed well. This also decreases V_{oc} to certain degree.[45-47] Under the combined actions of these two factors, V_{oc} remains stable after back interface passivation for ultrathin CIGSe solar cells on Mo.

Conclusion

In this work, we comparatively study the effect of SiO_2 point contact passivation layers in ultrathin CIGSe solar cells on Mo and ITO back contact. The SiO_2 passivation layer improves the cell performance with a relative efficiency enhancement by 16% for the cells on Mo. In contrast, cells on ITO exhibit a reverse evolution trend, implying that the back passivation is not desirable. Two factors are responsible for the sharp contrast. Optically, the SiO_2 point contact passivation layer improves the back reflectivity of CIGSe/Mo and leads to an absorption increment, which is negligible for the interface of CIGSe/ITO. Electrically, the passivation layer reduces the recombination of photogenerated carriers, which is beneficial for CIGSe solar cells. However, both theoretical and experimental results imply that the back passivation also aggravates the current limitation for solar cells with a Schottky back contact, as the passivation layer can suppress the hole transport to the back contact via recombination. It appears that recombination is an important method for carrier transport when E_h takes a non-negligible value. Since CIGSe solar cells on Mo have a small E_h, the electrical benefits of the SiO_2 outweigh the unfavorable ones. As E_h on ITO is relatively high, the aggravated current blocking effect prevails the benefits. Consequently, back interface passivation enhances the performance for cells on Mo and deteriorates it for cells on ITO. Those findings can support further understanding of the carrier transport mechanism in ultrathin CIGSe solar cells with ITO back contact.

Supporting information

Table S1: equivalent absorption current on Mo and ITO; Table S2: PV parameters of different contact ratios; Table S3: Model parameters for SCAPS simulation; Figure S1: GD-OES depth distribution of the Cu and Ga ratio; Figure S2: PV parameters of different S_b dependent on different E_h.

Acknowledgement

All authors would like to express their sincere gratitude to Klaus Pärschke and Tristan Köhler for technical support. The XRF measurement were performed on an instrument funded by the Deutsche Forschungsgemeinschaft (DFG, German Research Foundation) – INST 20876/324-1

FUGG and are acknowledged as follows: “Gefördert durch die Deutsche Forschungsgemeinschaft (DFG) – Projektnummer INST 20876/324-1 FUGG”. Yong Li receives the subsidy from the Chinese Scholarship Committee, Ye Tu and Guanchao Yin acknowledge the funding from the National Natural Science Foundation of China (NSFC, 51802240).

References

1. Nakamura, M.; Yamaguchi, K.; Kimoto, Y.; Yasaki, Y.; Kato, T.; Sugimoto, H., Cd-Free $Cu(In,Ga)(Se,S)_2$ Thin-Film Solar Cell with Record Efficiency of 23.35%. IEEE J. Photovoltaics 2019, 9 (6), 1863-1867.
2. Abou-Ras, D.; Wagner, S.; Stanbery, B. J.; Schock, H.-W.; Scheer, R.; Stolt, L.; Siebentritt, S.; Lincot, D.; Eberspacher, C.; Kushiya, K.; Tiwari, A. N., Innovation Highway: Breakthrough Milestones and Key Developments in Chalcopyrite Photovoltaics From a Retrospective Viewpoint. Thin Solid Films 2017, 633, 2-12.
3. Feurer, T.; Reinhard, P.; Avancini, E.; Bissig, B.; Löckinger, J.; Fuchs, P.; Carron, R.; Weiss, T. P.; Perrenoud, J.; Stutterheim, S.; Buecheler, S.; Tiwari, A. N., Progress in Thin Film CIGS Photovoltaics - Research and Development, Manufacturing, and Applications. Prog. Photovoltaics Res. Appl. 2017, 25 (7), 645-667.
4. Ramanujam, J.; Singh, U. P., Copper Indium Gallium Selenide Based Solar Cells – a review. Energy Environ. Sci. 2017, 10 (6), 1306-1319.
5. Wang, Y.-C.; Wu, T.-T.; Chueh, Y.-L., A Critical Review on Flexible $Cu(In, Ga)Se_2$ (CIGS) Solar Cells. Materials Chemistry and Physics 2019, 234, 329-344.
6. Ochoa, M.; Buecheler, S.; Tiwari, A. N.; Carron, R., Challenges and Opportunities for An Efficiency Boost of Next Generation $Cu(In,Ga)Se_2$ Solar Cells: Prospects for a Paradigm Shift. Energy Environ. Sci. 2020, 13 (7), 2047-2055.
7. Massiot, I.; Cattoni, A.; Collin, S., Progress and Prospects for Ultrathin Solar Cells. Nature Energy 2020, 5 (12), 959-972.
8. Mansfield, L. M.; Kanevce, A.; Harvey, S. P.; Bowers, K.; Beall, C.; Glynn, S.; Repins, I. L., Efficiency Increased to 15.2% for Ultra-thin Cu(In,Ga)Se2 Solar Cells. Prog. Photovoltaics Res. Appl. 2018, 1-6.
9. Yin, G.; Song, M.; Duan, S.; Manley, P.; Greiner, D.; Kaufmann, C. A.; Schmid, M., Well-Controlled Dielectric Nanomeshes by Colloidal Nanosphere Lithography for Optoelectronic Enhancement of Ultrathin $Cu(In,Ga)Se_2$ Solar Cells. ACS Appl Mater Interfaces 2016, 8 (46), 31646-31652.
10. Ohm, W.; Riedel, W.; Aksünger, Ü.; Greiner, D.; A, C.; Kaufmann; Ch, M.; Lux-Steiner; Gledhill, S., Bifacial $Cu(In,Ga)Se_2$ Solar Cells with Submicron Absorber Thickness: Back-contact Passivation and Light Management. In Photovoltaic Specialist Conference (PVSC), 2015; pp 1-5.
11. Vermang, B.; Wätjen, J. T.; Fjällström, V.; Rostvall, F.; Edoff, M.; Gunnarsson, R.; Pilch, I.; Helmersson, U.; Kotipalli, R.; Henry, F.; Flandre, D., Highly Reflective Rear Surface Passivation Design for Ultra-thin $Cu(In,Ga)Se_2$ Solar Cells. Thin Solid Films 2015, 582, 300-303.
12. Casper, P.; Hünig, R.; Gomard, G.; Kiowski, O.; Reitz, C.; Lemmer, U.; Powalla, M.; Hetterich, M., Optoelectrical Improvement of Ultra-thin $Cu(In,Ga)Se_2$ Solar Cells Through Microstructured MgF_2 and Al_2O_3 Back Contact Passivation Layer. physica status solidi (RRL) - Rapid Research Letters 2016, 10 (5), 376-380.
13. Bose, S.; Cunha, J. M. V.; Suresh, S.; De Wild, J.; Lopes, T. S.; Barbosa, J. R. S.;

Silva, R.; Borme, J.; Fernandes, P. A.; Vermang, B.; Salomé, P. M. P., Optical Lithography Patterning of SiO_2 Layers for Interface Passivation of Thin Film Solar Cells. Solar RRL 2018, 2 (12), 1800212.
14. Cunha, J. M. V.; Fernandes, P. A.; Hultqvist, A.; Teixeira, J. P.; Bose, S.; Vermang, B.; Garud, S.; Buldu, D.; Gaspar, J.; Edoff, M.; Leitao, J. P.; Salome, P. M. P., Insulator Materials for Interface Passivation of Cu(In,Ga)Se_2 Thin Films. IEEE J. Photovoltaics 2018, 8 (5), 1313-1319.
15. Garud, S.; Gampa, N.; Allen, T. G.; Kotipalli, R.; Flandre, D.; Batuk, M.; Hadermann, J.; Meuris, M.; Poortmans, J.; Smets, A.; Vermang, B., Surface Passivation of CIGS Solar Cells Using Gallium Oxide. physica status solidi (a) 2018, 215 (7), 1700826.
16. Ledinek, D.; Donzel-Gargand, O.; Sköld, M.; Keller, J.; Edoff, M., Effect of Different Na Supply Methods on Thin Cu(In,Ga)Se_2 Solar Cells With Al_2O_3 Rear Passivation Layers. Sol. Energy Mater. Sol. Cells 2018, 187, 160-169.
17. Lopes, T. S.; Cunha, J. M. V.; Bose, S.; Barbosa, J. R. S.; Borme, J.; Donzel-Gargand, O.; Rocha, C.; Silva, R.; Hultqvist, A.; Chen, W.-C.; Silva, A. G.; Edoff, M.; Fernandes, P. A.; Salome, P. M. P., Rear Optical Reflection and Passivation Using a Nanopatterned Metal/Dielectric Structure in Thin-Film Solar Cells. IEEE J. Photovoltaics 2019, 9 (5), 1421-1427.
18. Schneider, T.; Tröndle, J.; Fuhrmann, B.; Syrowatka, F.; Sprafke, A.; Scheer, R., Ultrathin CIGSe Solar Cells with Integrated Structured Back Reflector. Solar RRL 2020, 4 (10), 2000295.
19. Kotipalli, R.; Poncelet, O.; Li, G.; Zeng, Y.; Francis, L. A.; Vermang, B.; Flandre, D., Addressing the Impact of Rear Surface Passivation Mechanisms on Ultra-thin Cu(In,Ga)Se_2 Solar Cell Performances Using SCAPS 1-D model. Sol. Energy 2017, 157, 603-613.
20. Cunha, J. M. V.; Oliveira, K.; Lontchi, J.; Lopes, T. S.; Curado, M. A.; Barbosa, J. R. S.; Vinhais, C.; Chen, W.-C.; Borme, J.; Fonseca, H.; Gaspar, J.; Flandre, D.; Edoff, M.; Silva, A. G.; Teixeira, J. P.; Fernandes, P. A.; Salomé, P. M. P., High-Performance and Industrially Viable Nanostructured SiO_x Layers for Interface Passivation in Thin Film Solar Cells. Solar RRL 2021, 5, 2000534.
21. Kotipalli, R.; Vermang, B.; Joel, J.; Rajkumar, R.; Edoff, M.; Flandre, D., Investigating the Electronic Properties of Al_2O_3/Cu(In,Ga)Se_2 Interface. AIP Advances 2015, 5 (10), 603-613.
22. Schmid, M.; Manley, P.; Ott, A.; Song, M.; Yin, G., Nanoparticles for Light Management in Ultrathin Chalcopyrite Solar Cells. Journal of Materials Research 2016, 31 (21), 3273-3289.
23. Schmid, M., Review on Light Management by Nanostructures in Chalcopyrite Solar Cells. Semiconductor Science and Technology 2017, 32 (4), 043003.
24. Kim, D.; Shin, S. S.; Lee, S. M.; Cho, J. S.; Yun, J. H.; Lee, H. S.; Park, J. H., Flexible and Semi-transparent Ultra-thin CIGSe Solar Cells Prepared on Ultra-thin Glass Substrate: a Key to Flexible Bifacial Photovoltaic Applications. Adv. Funct. Mater. 2020, 2001775.
25. Li, Y.; Yin, G.; Gao, Y.; Köhler, T.; Lucaßen, J.; Schmid, M., Sodium Control in Ultrathin Cu(In,Ga)Se_2 Solar Cells on Transparent Back Contact for Efficiencies Beyond 12%. Sol. Energy Mater. Sol. Cells 2021, 223, 110969.
26. Gouillart, L.; Cattoni, A.; Chen, W. C.; Goffard, J.; Riekehr, L.; Keller, J.; Jubault, M.; Naghavi, N.; Edoff, M.; Collin, S., Interface Engineering of Ultrathin Cu(In,Ga)Se_2 Solar Cells on Reflective Back Contacts. Prog. Photovoltaics Res. Appl. 2020, 29, 212-221.
27. Shin, M. J.; Jo, J. H.; Cho, A.; Gwak, J.; Yun, J. H.; Kim, K.; Ahn, S. K.; Park, J. H.; Yoo, J.; Jeong, I.; Choi, B.-H.; Cho, J.-S., Semi-transparent Photovoltaics Using Ultra-thin Cu(In,Ga)Se_2 Absorber Layers Prepared by Single-stage Co-evaporation. Sol. Energy

2019, 181, 276-284.
28. Shin, M. J.; Lee, A.; Cho, A.; Kim, K.; Ahn, S. K.; Park, J. H.; Yoo, J.; Yun, J. H.; Gwak, J.; Shin, D.; Jeong, I.; Cho, J.-S., Semitransparent and Bifacial Ultrathin Cu(In,Ga)Se_2 Solar Cells via a Single-stage Process and Light-management Strategy. Nano Energy 2021, 82, 105729.
29. Saifullah, M.; Kim, D.; Cho, J.-S.; Ahn, S.; Ahn, S.; Yun, J. H.; Lee, H. S.; Park, J. H., The role of NaF Post-deposition Treatment on the Photovoltaic Characteristics of Semitransparent Ultrathin Cu(In,Ga)Se_2 Solar Cells Prepared on Indium-tin-oxide Back Contacts: A Comparative Study. J. Mater. Chem. A 2019, 7 (38), 21843-21853.
30. Saifullah, M.; Rasool, S.; Ahn, S.; Kim, K.; Cho, J. S.; Yoo, J. S.; Shin, W. S.; Yun, J. H.; Park, J. H., Performance and Uniformity Improvement in Ultrathin Cu(In,Ga)Se_2 Solar Cells with a WO_x Nano-Interlayer at the Absorber/Transparent Back-Contact Interface. ACS Applied Materials and Interfaces 2019, (11), 655-665.
31. Tu, Y.; Li, Y.; Klenk, R.; Yin, G.; Schmid, M., Is a Passivated Back Contact Always Beneficial for Cu (In,Ga)Se_2 Solar Cells. Prog. Photovoltaics Res. Appl. 2021, 1-8.
32. Yin, G.; Brackmann, V.; Hoffmann, V.; Schmid, M., Enhanced Performance of Ultra-thin Cu(In,Ga)Se_2 Solar Cells Deposited at Low Process Temperature. Sol. Energy Mater. Sol. Cells 2015, 132, 142-147.
33. Decock, K.; Khelifi, S.; Buecheler, S.; Pianezzi, F.; Tiwari, A. N.; Burgelman, M., Defect Distributions in Thin Film Solar Cells Deduced From Admittance Measurements Under Different Bias Voltages. J. Appl. Phys. 2011, 110 (6).
34. Decock, K.; Khelifi, S.; Burgelman, M., Modelling Multivalent Defects in Thin Film Solar Cells. Thin Solid Films 2011, 519 (21), 7481-7484.
35. Burgelman, M.; Decock, K.; Khelifi, S.; Abass, A., Advanced Electrical Simulation of Thin Film Solar Cells. Thin Solid Films 2013, 535, 296-301.
36. Decock, K.; Khelifi, S.; Burgelman, M., Modelling and Measurement of the Metastable Defect Distribution in Chalcopyrite-based Thin Film Solar Cells. Thin Solid Films 2013, 535, 362-365.
37. Sze, S. M.; Ng, K. K., Physics of Semiconductor Devices. John Wiley & Sons: Hoboken, New Jersey. Published simutaneously in Canada., 2007, Chapter 1, p68.
38. Salomé, P. M. P.; Vermang, B.; Ribeiro-Andrade, R.; Teixeira, J. P.; Cunha, J. M. V.; Mendes, M. J.; Haque, S.; Borme, J.; Águas, H.; Fortunato, E.; Martins, R.; González, J. C.; Leitão, J. P.; Fernandes, P. A.; Edoff, M.; Sadewasser, S., Passivation of Interfaces in Thin Film Solar Cells: Understanding the Effects of a Nanostructured Rear Point Contact Layer. Advanced Materials Interfaces 2018, 5 (2), 1701101.
39. Manley, P.; Yin, G.; Schmid, M., A method for Calculating the Complex Refractive Index of Inhomogeneous Thin Films. Journal of Physics D: Applied Physics 2014, 47 (20), 205301.
40. Rebecca, S., S-Shaped Current–Voltage Characteristics in Solar Cells: A Review. IEEE J. Photovoltaics 2019, 9 (6), 1477-1484.
41. Hegedus, S. S.; Shafarman, W. N., Thin-film Solar Cells: Device Measurements and Analysis. Prog. Photovoltaics Res. Appl. 2004, 12 (23), 155-176.
42. Chirila, A.; Buecheler, S.; Pianezzi, F.; Bloesch, P.; Gretener, C.; Uhl, A. R.; Fella, C.; Kranz, L.; Perrenoud, J.; Seyrling, S.; Verma, R.; Nishiwaki, S.; Romanyuk, Y. E.; Bilger, G.; Tiwari, A. N., Highly Efficient Cu(In,Ga)Se_2 Solar Cells Grown on Flexible Polymer Films. Nat Mater 2011, 10 (11), 857-61.
43. Hsiao, K. J.; Liu, J. D.; Hsieh, H. H.; Jiang, T. S., Electrical Impact of $MoSe_2$ on CIGS Thin-film Solar Cells. Phys Chem Chem Phys 2013, 15 (41), 18174-8.
44. Zhang, X.; Kobayashi, M.; Yamada, A., Comparison of Ag(In,Ga)Se_2/Mo and Cu(In,Ga)Se_2/Mo Interfaces in Solar Cells. ACS Appl Mater Interfaces 2017, 9 (19), 16215-

16220.
45. Abou-Ras, D.; Kostorz, G.; Bremaud, D.; Kälin, M.; Kurdesau, F.V.; Tiwari, A.N.; Döbeli, M., Formation and Characterisation of $MoSe_2$ for Cu(In, Ga)Se_2 Based Solar Cells. Thin Solid Films 2005, 480, 433-438.
46. Kohara, N.; Nishiwaki, S.; Hashimoto, Y.; Negami, T.; Wada, T., Electrical Properties of the Cu(In, Ga)Se_2/$MoSe_2$/Mo Structure. Sol. Energy Mater. Sol. Cells 2001, 67, 209-215.
47. Hsiao, K.; Liu, J., Hsieh, H.; Jiang, T., Electrical Impact of $MoSe_2$ on CIGS Thin-film Solar Cells. Phys. Chem. Chem. Phys., 2013, 15, 18174-18178

Table of Content graphic

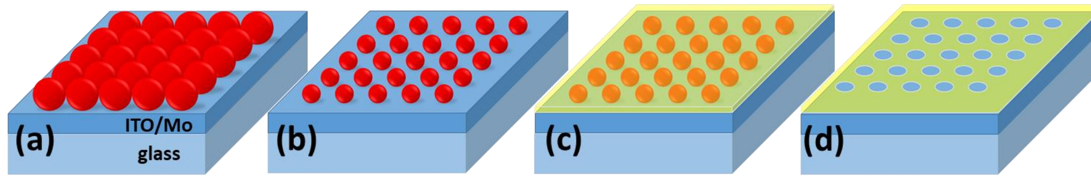

Figure 1. Fabrication steps of SiO_2 point contact passivation layers: (a) deposition of polystyrene (PS) spheres, (b) plasma etching, (c) SiO_2 deposition, (d) PS mask liftoff.

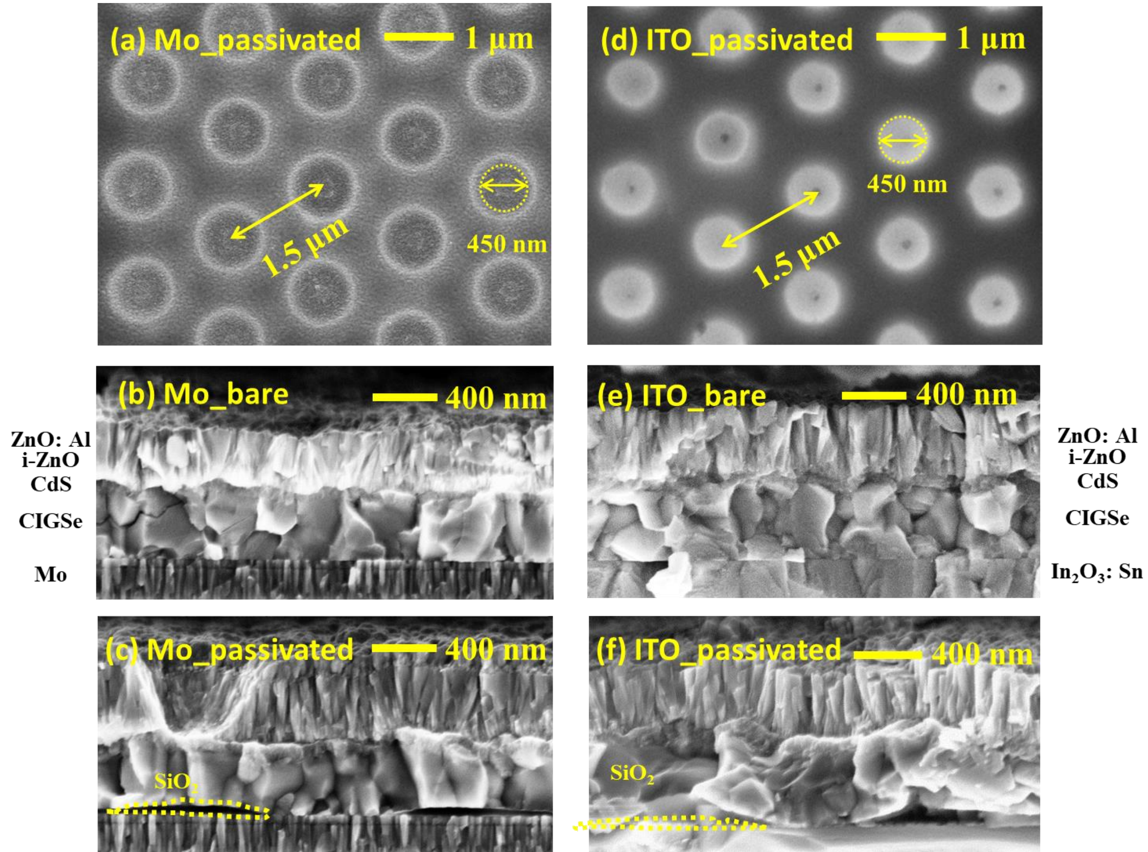

Figure 2. Top views of SiO_2 point contact passivation layers and cross-sections of ultrathin CIGSe solar cells without (_bare) and with (_passivated) point contacts: (a)-(c) on Mo and (d)-(f) on ITO

Table 1. PV parameters of ultrathin CIGSe solar cells on Mo and ITO without (_bare) and with (_passivated) SiO_2 point contact passivation layers

Sample name	V_{oc} (mV)	j_{sc} (mA/cm^2)	FF (%)	Eff (%)	R_{sh} (Ωcm^2)	R_s (Ωcm^2)
Mo_bare	609	25.3	61.8	9.5	250	0.6
Mo_passivated	609	28.2	64.5	11.1	500	1.7
ITO_bare	596	26.6	59.9	9.5	333	3.6
ITO_passivated	574	26.9	58.0	9.0	3333	5.4

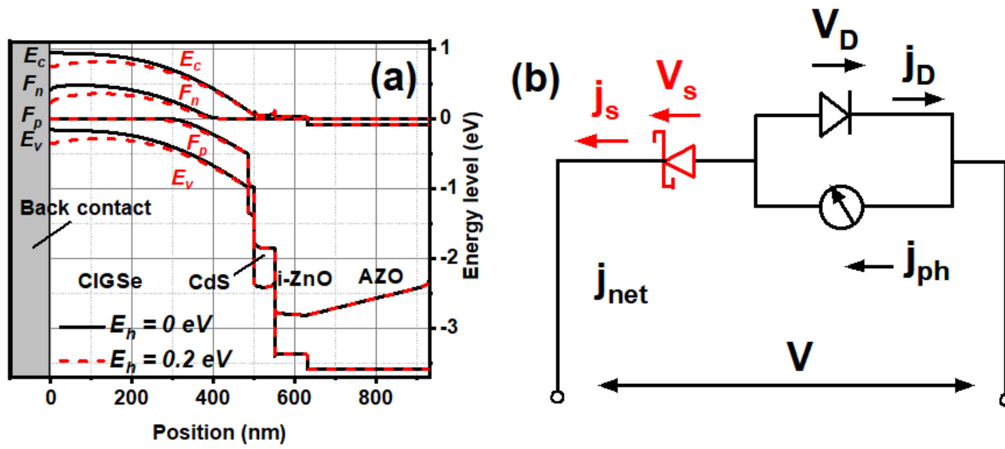

Figure 3. (a) Band diagram of the device with Ohmic contact (black line E_h = 0 eV) and Schottky contact (red dotted line, E_h = 0.2 eV) at zero bias voltage calculated in SCAPS and (b) the corresponding equivalent circuit with additional Schottky diode marked in red.

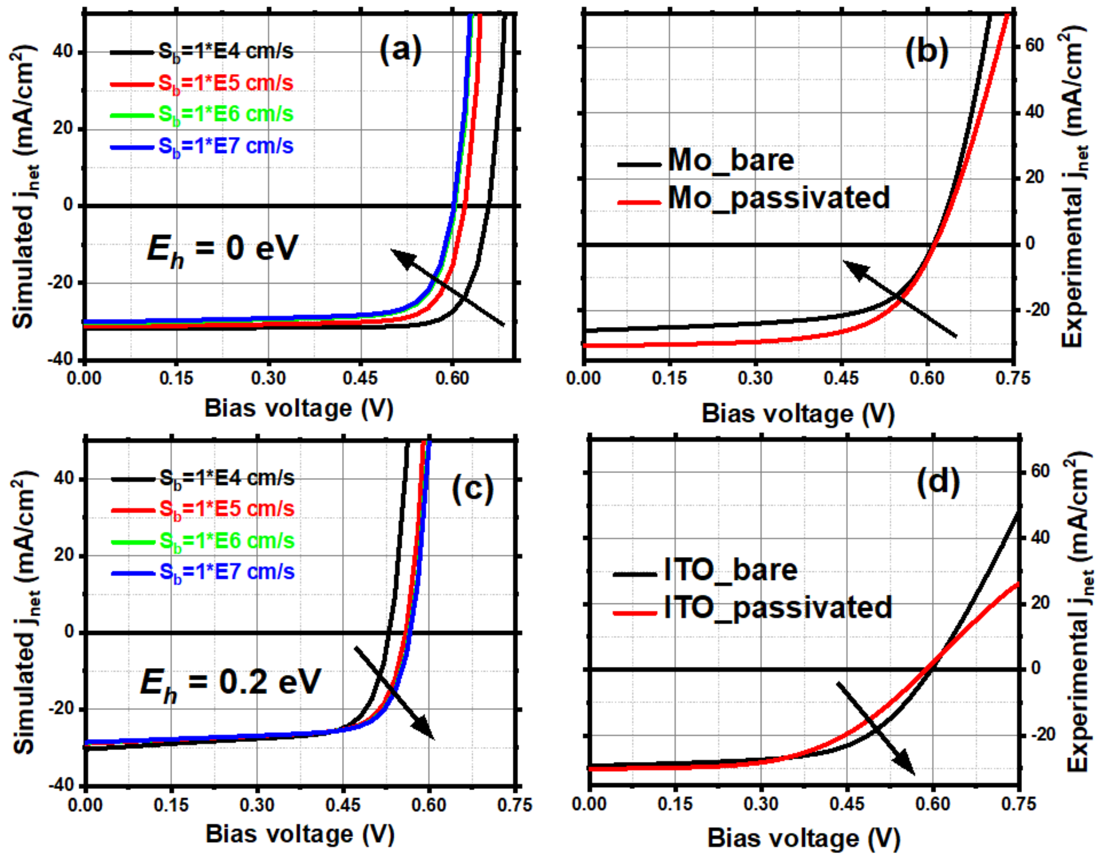

Figure 4. Simulated $j_{net}V$ curves of solar cells with (a) Ohmic (E_h = 0 eV) and (c) Schottky (E_h = 0.2 eV) contact as a function of recombination velocity S_b. Simulation details of each layer are listed in Table S2. Experimental $j_{net}V$ characteristics of ultrathin CIGSe solar cells under illumination on (b) Mo and (d) ITO. The black arrow marks the direction of increasing S_b.

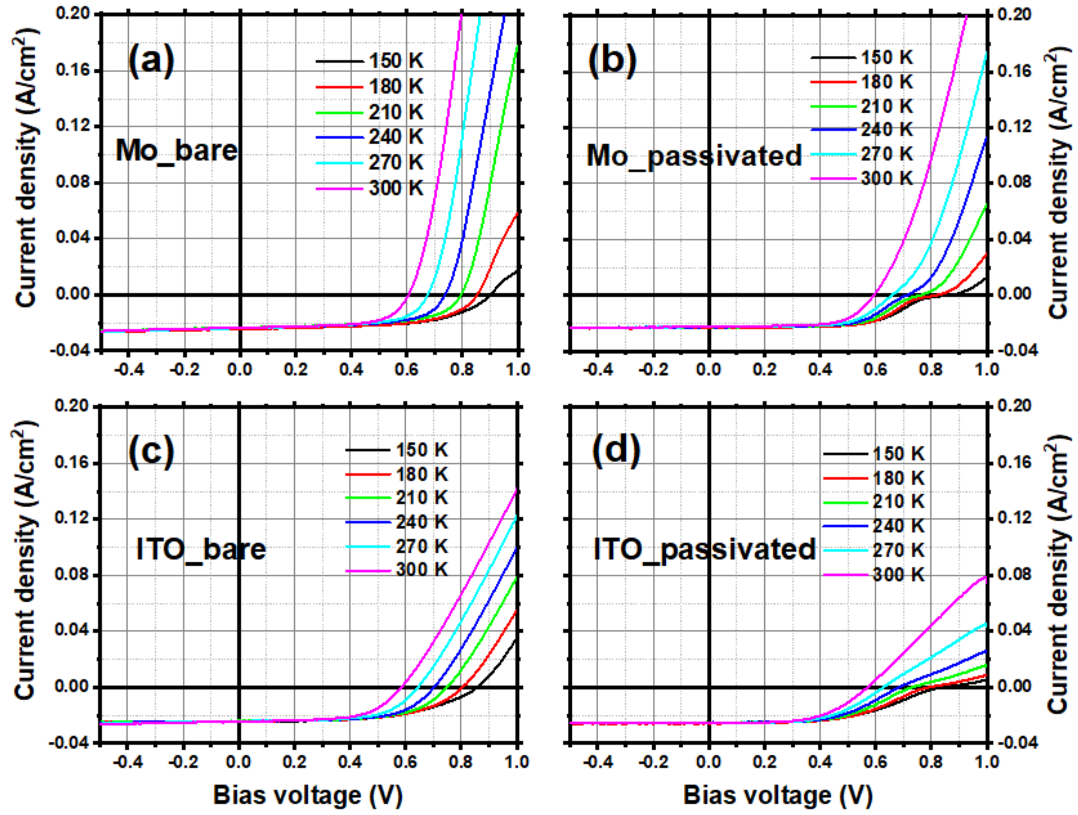

Figure 5. Temperature-dependent current-voltage properties of representative ultra-thin CIGSe solar cells on Mo (a) without Mo_bare and (b) with SiO_2 passivation layer Mo_passivated; On ITO substrates (c) without ITO_bare and (d) with SiO_2 passivation layer ITO_passivated.

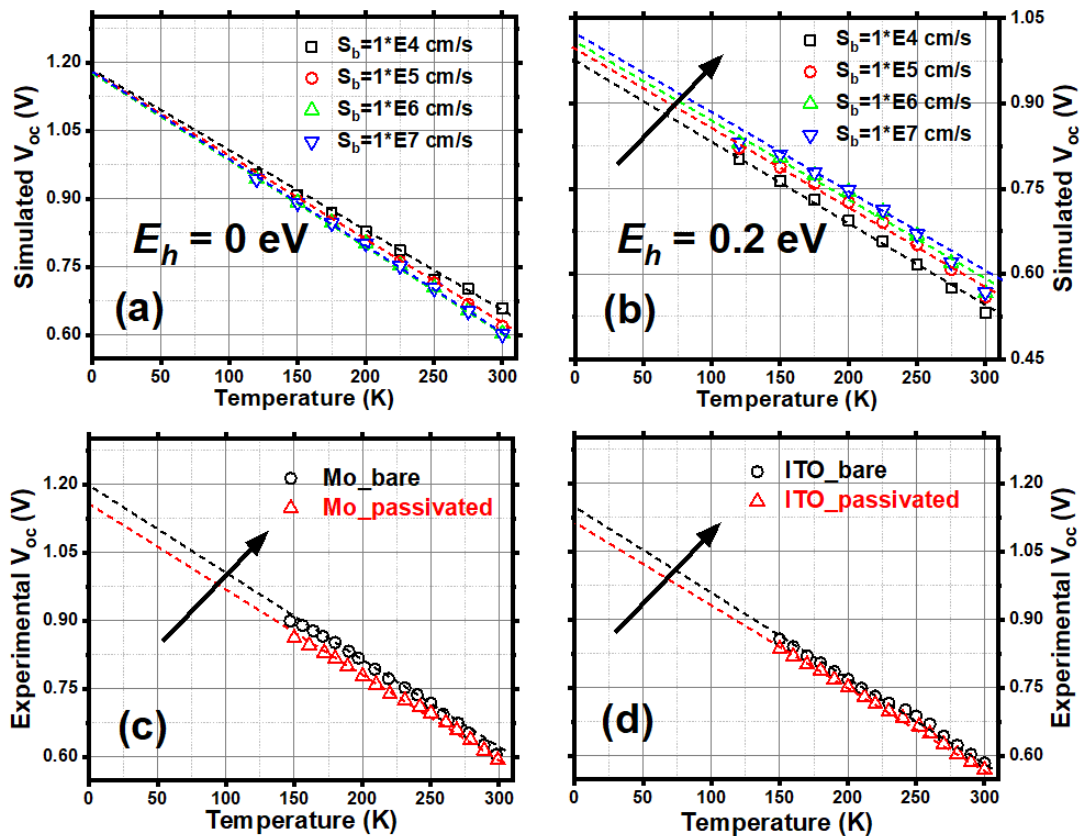

Figure 6. SCAPS simulated temperature-dependent V_{oc} at varied S_b for (a) Ohmic (E_h = 0 eV) and (b) Schottky (E_h = 0.2 eV) back contact. and experimental temperature-dependent $V_{oc}(T)$ for CIGSe solar cells on (c) Mo and (d) ITO. Arrows indicate the direction of increasing S_b.

Graphic abstract